

Omni-AD: Learning to Reconstruct Global and Local Features for Multi-class Anomaly Detection

Jiajie Quan¹, Ao Tong², Yuxuan Cai², Xinwei He^{1†}, Yulong Wang¹, Yang Zhou³

¹Huazhong Agricultural University

²Huazhong University of Science and Technology

³Shenzhen University

Abstract—In multi-class unsupervised anomaly detection (MUAD), reconstruction-based methods learn to map input images to normal patterns to identify anomalous pixels. However, this strategy easily falls into the well-known “learning shortcut” issue when decoders fail to capture normal patterns and reconstruct both normal and abnormal samples naively. To address that, we propose to learn the input features in global and local manners, forcing the network to memorize the normal patterns more comprehensively. Specifically, we design a two-branch decoder block, named Omni-block. One branch corresponds to global feature learning, where we serialize two self-attention blocks but replace the query and (key, value) with learnable tokens, respectively, thus capturing global features of normal patterns concisely and thoroughly. The local branch comprises depth-separable convolutions, whose locality enables effective and efficient learning of local features for normal patterns. By stacking Omni-blocks, we build a framework, Omni-AD, to learn normal patterns of different granularity and reconstruct them progressively. Comprehensive experiments on public anomaly detection benchmarks show that our method outperforms state-of-the-art approaches in MUAD. Code is available at <https://github.com/easyoo/Omni-AD.git>

Index Terms—unsupervised image anomaly detection, reconstruction, depth convolution, self-attention

I. INTRODUCTION

The past decade has witnessed the rapid development of smart manufacturing. Within this realm, Visual Anomaly Detection (VAD) has emerged as an essential component. Given the difficulty in collecting and labeling anomaly data, previous work operates mainly in an unsupervised manner, such as Embedding-based [1], Synthesizing-based [2], and Reconstruction-based [3]. However, these works are mostly in a single-class setting [4], where a separate VAD model needs to be trained using only normal training images for each product category. More recently, multi-class unsupervised anomaly detection (MUAD) has been introduced and has drawn researchers’ great attention [3], [5]. It only needs to train a unified model with normal images of N categories at once, making it more practical and efficient.

Existing MUAD research mainly focuses on reconstruction strategy. They primarily use a pre-trained backbone to extract features and then train a unified decoder to reconstruct the input with learned *normal* patterns. Anomalous pixels can be identified by comparing the input and output. However, to map any input to its normal counterparts, a model has to

comprehensively encapsulate both local and global features of diverse normal samples across distinct categories. Take MVTec-AD [6] as an example: the decoder is expected to learn *local* repetitive normal patterns in texture classes but also understand the *global* structural integrity of object classes. This poses great challenges to existing methods, as decoders can learn to take “shortcuts” in training. One way is to build the decoder using the attention mechanism [7] to capture long-range dependency. Yet, it is still at the risk of learning “shortcuts”, as the query, key and value from self-attention are coupled with input. UniAD [3] replaces the query with learnable tokens, forcing them to learn normal pattern distributions. RLR [8] choose to replace key and value with learnable ones. Yet they all lack sufficient capacity to learn local normal features. As we know, convolutions are good at extracting fine-grained local spatial features. *Could we build a decoder with self-attention and convolution, to comprehensively learn both local and global normal patterns?*

Motivated by this, we design a two-branch decoding block named Omni-block with one global branch implemented by modified self-attention with learnable tokens and the other local branch implemented by convolution. The global branch aims to fully decouple the query, key, and value from the input with two multi-head attention blocks. To avoid the “learning shortcut”, we sequentially alternate the decoupling of query and (key, value) with extra learnable tokens. The parallel local branch is implemented by depth-wise separable convolutions to effectively and efficiently learn fine-grained local normal features. By combining both outputs, we combine the merits of locality in convolution and global relations in MUAD setups. Besides, due to the minimal size of learnable tokens in attention, we are able to reduce the computational complexity to be linear with the size of inputs, which makes our network very efficient at handling high-resolution inputs. Then, with this dual branch block, we develop a framework named **Omni-AD** to progressively learn to reconstruct multi-scale normal features, which comprehensively captures both long-range dependencies and different granularities of normal patterns. Empirical results on several popular VAD benchmarks show that our framework has obtained remarkable improvements over state-of-the-art methods in the MUAD setting.

Our contributions are summarized as follows:

- We propose a two-branch block named Omni-block, which mitigates “learning shortcut” issues and efficiently

[†]Corresponding author (Email: xwhe@mail.hzau.edu.cn)

learns both global and local normal features.

- We develop Omni-AD upon Omni-blocks to capture different granularities of normal patterns, progressively mapping an input to a normal output.
- Extensive experiments on various popular VAD benchmarks demonstrate the validity and superiority of our design in the MUAD setting.

II. RELATED WORK

Unsupervised Anomaly Detection. Mainstream anomaly detection methods can be broadly categorized into three types: *embedding-based*, *synthesizing-based*, and *reconstruction-based* approaches. 1) **Embedding-based methods** [1] leverage pre-trained models to extract features of normal samples and identify anomalies by statistically analyzing deviations in the embedding space. For instance, PatchCore [1] utilizes a memory bank to store normal patch features and measures Mahalanobis distance between test sample features and normal features from the memory bank. FastFlow [9] employs a 2D flow model to estimate probability distributions and detect anomalies, preserving the spatial relationships of features. PaDim [10] utilizes multivariate Gaussian distributions to model the normal embedding space. However, these works typically require heavy resources and are unfriendly for real-time applications. 2) **Synthesizing-based methods** [2] focus on simulating anomalous regions to generate pseudo-supervisory masks, which helps the model learn to differentiate normal and abnormal distributions. For example, DRAEM [2] generates anomalous regions by embedding diverse masks from other images into normal samples. CutPaste [11] cuts an image patch and pasts it to another image for training. DAF [12] further improves the robustness of existing works by taking discrepancy-aware maps for synthesizing-based methods. However, these methods have a heavy reliance on the quality of synthesized schemes. Besides, anomalies are unknown, and synthesizing all types of anomalies is impossible. 3) **Reconstruction-based methods** aim to restore anomalous pixels or features to their corresponding normal representations. Models such as Autoencoder [13], Generative Adversarial Networks (GANs) [14], diffusion models [15] and Transformer [16] have been widely utilized. Based on the generation quality, anomaly maps can be easily derived by comparing the input and the reconstructed output. However, it has been shown that these methods face the “learning shortcuts” and sometimes well-restore the anomalies, failing to spot the anomalies by comparisons. Our method also belongs to this category, but we attempt to alleviate this issue by designing a suitable hybrid decoder with self-attention and depth convolution, forcing the model to focus on comprehensively learning both local and global normal patterns instead of shortcuts.

Multi-class Anomaly Detection. The seminal work UniAD [3] presents the learnable query to alleviate the shortcut issues in reconstruction-based methods. OmniAL [17] trains a unified model using panel-guided synthetic anomaly data instead of relying solely on normal data. Similarly,

HVQ-Trans [18] employs a hierarchical codebook mechanism to mitigate shortcut learning. Additionally, diffusion model demonstrates strong performance [19]. RLR [8] proposes to decouple the key and value from the input. In contrast, we incorporate attention with learnable tokens to *fully* detach the query, key, and value. Besides, we also incorporate convolution to enhance the learning of local normal patterns, ensuring a more accurate multi-class anomaly detection.

III. METHOD

A. Network Architecture

Figure 1 gives an overview of the proposed Omni-AD. As shown, it has three main components: a feature extractor, a feature fusion neck, and a decoder. We elaborate each below.

Feature Extractor. Given an input image $I \in \mathbb{R}^{H \times W \times 3}$, we first feed it into a pretrained CNN $\Phi(\cdot)$ to extract its multi-scale features. Any off-the-shelf CNN pretrained on large-scale datasets like ImageNet [20] can be utilized as the feature extractor, such as ResNet [21] and EfficientNet [22]. In this paper, we follow [5] and utilize ResNet34 [21], which has several feature encoding stages to derive feature maps of decreasing resolution. Assuming that \mathcal{L} contains the selected hierarchical stage index subset of $\Phi(\cdot)$ for use, we can denote feature maps of level $l \in \mathcal{L}$ as $\Phi^l \sim \Phi(I_i)^l \in \mathbb{R}^{H_l \times W_l \times C_l}$, where H_l , W_l and C_l represent are the height, width, and channel dimensions of the feature maps. In our framework, following [5], we only use outputs of the last three stages, denoted as $\mathcal{L} = \{\Phi^{l_k}\}_{k=1}^3$, with $\Phi^{l_k} \in \mathbb{R}^{\frac{H}{2^{k+1}} \times \frac{W}{2^{k+1}} \times 2^{k-1}C}$.

Feature Fusion Neck. We aggregate $\{\Phi^{l_k}\}_{k=1}^3$, the feature maps at different hierarchical levels, by feeding them to an H-FPN-style feature fusion neck [23]. The neck consists of several CBR blocks (Conv+BN+ReLU) and one bottleneck layer for progressive fusion. As shown, given $\{\Phi^{l_k}\}_{k=1}^3$, it first integrate Φ^{l_1} with Φ^{l_2} . Next, the fused features are combined with Φ^{l_3} . Finally, the bottleneck layer is utilized to double the channel dimensions while halving the spatial ones, giving combined features $\Phi^{\text{final}} \in \mathbb{R}^{\frac{H}{32} \times \frac{W}{32} \times 8C}$. Since $\{\Phi^{l_k}\}_{k=1}^3$ have different resolutions, each pixel location in the resulting Φ^{final} collects different scales of contextual information.

Decoder. The fused feature maps Φ^{final} are further fed into the decoder, which is composed of four stages, with each stage i comprising M_i Omni-blocks (see Sec. III-B). Between these stages, we incorporate upsampling layers to progressively restore the multi-scale spatial resolutions for reconstruction. We adopt feature maps at the last three stages, denoted by $\{\hat{\Phi}^{l_k}\}_{k=1}^3$. Finally, we train it with mean squared error (MSE) by summing up reconstruction errors across the three scales.

B. Omni-block

As illustrated in Figure 2, our Omni-block is a two-branch module. One branch is designed to learn global relations through two multi-head attention modules. In this branch, learnable tokens are utilized to replace the query (Q), key (K) and value (V) alternatively, making it efficiently learn global normal features while avoiding the “learning shortcut”

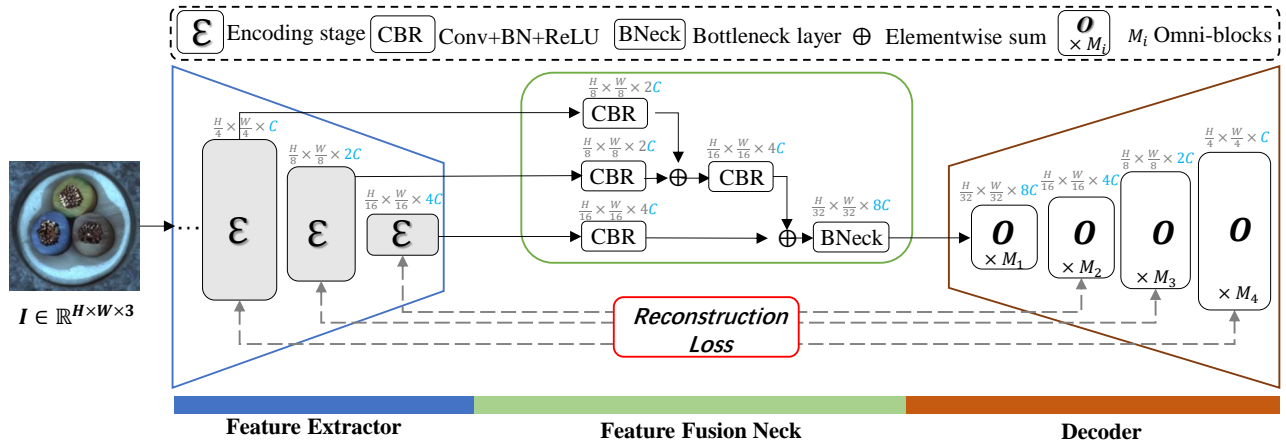


Fig. 1. Overview of Omni-AD. Given an input image, we first use a pretrained network to extract its multi-scale features. Then, we fuse them with the feature fusion neck. Finally, we feed it into the decoder comprising a series of Omni-blocks to reconstruct multi-scale features progressively.

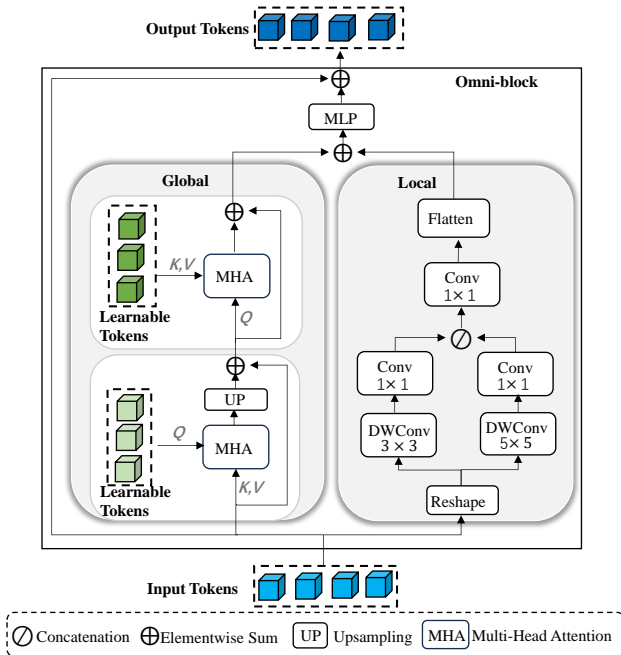


Fig. 2. Detailed structure of the proposed Omni-block.

issue. The other branch learns local features with convolutions, capturing fine-grained normal patterns effectively. Let $\mathbf{X} \in \mathbb{R}^{N \times D}$ denote the input features, where N is the input token number and D is the token dimension. The computing process of Omni-block is described as follows.

Global branch with learnable tokens. First, we feed \mathbf{X} to the global branch, which consists of two multi-head attention blocks (MHA). Each MHA [7] is just a plain self-attention module, taking Query Q , Key K , Value V as input:

$$\text{MHA}(Q, K, V) = \text{Concat}(\text{head}_1, \dots, \text{head}_H)W^O$$

$$\text{where } \text{head}_i = \text{softmax}\left(\frac{QW_i^Q(KW_i^K)^T}{\sqrt{D_h}}\right)VW_i^V \quad (1)$$

where H is head number, and i is the index, $W_i^Q, W_i^K, W_i^V \in \mathbb{R}^{D \times D_h}$ are weight matrices to project Q, K and V for each head, and $W^O \in \mathbb{R}^{HD_h \times D}$ are parameter matrix with $HD_h = D$. In standard self-attention [7], the (Q, K, V) triplet are typically the input features \mathbf{X} , which are tightly-coupled to the output and easily leads to the “learning shortcuts” issue [3]. To alleviate this issue, we propose to alternately replace $Q, (K, V)$ with learnable tokens, respectively, for decoupling.

For the first MHA, we use learnable tokens $\bar{Q} \in \mathbb{R}^{T \times D}$ to harvest context information in the input \mathbf{X} , i.e., $\mathbf{F}_1 = \text{MHA}(\bar{Q}, \mathbf{X}, \mathbf{X}) \in \mathbb{R}^{T \times D}$. Note that \bar{Q} is optimized to capture the normal distributions during training. As a result, it is difficult to reconstruct abnormal samples. Another benefit is that T is much smaller than input size N , which decreases the key-query dot product complexity from $\mathcal{O}(N^2D)$ to be linear in the input size $\mathcal{O}(NTD)$, and thus is more efficient. Finally, we upsample \mathbf{F}_1 with $\text{Up}(\cdot)$ and add a residual connection with input X , i.e., $\mathbf{Y}_1 = \text{Up}(\mathbf{F}_1) + \mathbf{X}, \mathbf{Y}_1 \in \mathbb{R}^{N \times D}$.

For the second MHA, we treat \mathbf{Y}_1 as the query Q which contains the information from \mathbf{X} , while key K and value V coming from shared learnable tokens $\bar{S} \in \mathbb{R}^{T \times D}$, i.e., $K, V = \bar{S}W^K, \bar{S}W^V$, where $W^K, W^V \in \mathbb{R}^{D \times D}$ are projection matrices. We finally feed them into MHA to learn normal distributions: $\mathbf{F}_2 = \text{MHA}(\mathbf{Y}_1, K, V)$. Note that the \bar{S} can be regarded as normal reference features during training. At the inference stage, the abnormal tokens deviate from these normal references, which is helpful for anomaly identification. Moreover, it is also efficient due to the linear computational complexity. Similarly, residual connections are incorporated, i.e., $\mathbf{Y}_2 = \mathbf{F}_2 + \mathbf{Y}_1, \mathbf{Y}_2 \in \mathbb{R}^{N \times D}$.

With the above two MHA, we can achieve the decoupling of Query, Key, and Value completely, thus effectively helping the model to understand normal patterns better.

Local branch with depth-separable convolution. Complementary to the global branch, a parallel local branch is utilized to enhance the locality information extraction. To this end, we simply adopt depth-wise convolution for the parameter

and computation efficiency. Specifically, we first reshape \mathbf{X} to restore its spatial size (h, w) : $\mathbf{X}' = \text{Reshape}(\mathbf{X}) \in \mathbb{R}^{h \times w \times D}$, where $N = hw$. After that, we use Depthwise Separable Convolution, which factorizes standard $k \times k$ convolution into $k \times k$ depth convolution $\text{DWConv}_{k \times k}$ and 1×1 point-wise convolution $\text{Conv}_{1 \times 1}$. We utilize two kernel sizes in parallel: 3×3 and 5×5 , and then combine the outputs with concatenation after padding and 1×1 convolution for channel reduction. Finally, we flatten the spatial dimensions. The process is formulated below:

$$\mathbf{F}_3 = \text{Conv}_{1 \times 1}(\text{DWConv}_{3 \times 3}(\mathbf{X}')) \quad (2)$$

$$\mathbf{F}_4 = \text{Conv}_{1 \times 1}(\text{DWConv}_{5 \times 5}(\mathbf{X}')) \quad (3)$$

$$\mathbf{F}_5 = \text{Flatten}(\text{Conv}_{1 \times 1}(\text{Cat}(\mathbf{F}_3, \mathbf{F}_4))) \quad (4)$$

The local branch facilitates the learning of local patterns.

Finally, we combine output from local and global branches.

$$\mathbf{O}_{\text{final}} = \text{MLP}(\mathbf{Y}_2 + \mathbf{F}_5) + \mathbf{X} \quad (5)$$

C. Training and Inference

For training, we utilize Mean Square Error to measure the loss between reconstructed features $\{\hat{\Phi}^{l_k}\}_{k=1}^3$ and the original extracted features $\{\Phi^{l_k}\}_{k=1}^3$. The loss function is defined as

$$\mathcal{L} = \sum_{k=1}^3 \frac{\|\Phi^{l_k} - \hat{\Phi}^{l_k}\|_2^2}{H_k W_k}, \quad (6)$$

For inference, we combine cosine similarities across multiple scales, specifically at 2, 3, and 4 stages, to derive the anomaly maps.

IV. EXPERIMENTS

A. Experimental Setup

Datasets. **MVTec-AD** [6] consists of 15 categories, including 5 texture types and 10 object types. It has 3,629 normal images for training, with 467 normal and 1,258 anomalous images for testing. **VisA** [24] has a total of 10,821 images divided into 12 objects, including 9,621 normal samples and 1,200 anomalous samples. **Real-IAD** [25] is largest industrial anomaly detection dataset. It comprises 30 distinct objects, with 36,465 normal images for training and 114,585 images for testing, including 63,256 normal and 51,329 anomalous samples.

Metric. Following [5], [26], we report Area Under the Receiver Operating Curve (AU-ROC) [2], Average Precision (AP) [2], and F1-score (F1_max) [24], at the image level. For pixel-level, we also report Area Under the Per-Region-Overlap (AU-PRO) [27]. We calculate the average anomaly detection score (mAD) [28] to assess overall performance.

Implementation Details. All input images are resized to 256×256 . Following MambaAD [5], we use a pre-trained ResNet-34 [21] for feature extraction. The decoder consists of four stages, with 3, 9, 9, and 7 Omni blocks stacked in each stage, respectively. Stages 2-4 start with spatial upsampling. We use AdamW with learning rate 1×10^{-3} and weight decay 1×10^{-4} and train for 500 epochs.

B. Main Results

We compare against MUAD methods, *i.e.*, UniAD [3], DiAD [19], RLR [8] and MambaAD [5]. We also compare with other superior reconstruction-based method RD4AD [29] and embedding-based ones (DeSTseg [30] and SimpleNet [4]).

As shown in Table I, on **MVTec-AD**, our approach outperforms all the compared methods. At the image level, it obtains detection performance of 99.0/99.7/98.3, and at the pixel level, it attains segmentation of 97.9/56.8/59.9/93.4. Specifically, compared with previous state-of-the-art method MambaAD, we achieve increases of 0.4/0.1/0.5 in detection and 0.2/0.5/0.7/0.3 in segmentation. The overall mAD metric improves by 0.4 and 2.4 when compared with MambaAD and DiAD, respectively. On the challenging **VISA** dataset, our method also attains the leading performance, where all our metrics significantly exceed DiAD, with mAD improving by 8.8. It also has a better average performance than MambaAD, improving mAD by 0.2. Finally, on the largest **Real-IAD** dataset, we remarkably surpass the best previous method MambaAD by 1.3% mAD. These results consistently demonstrate the superiority of the proposed Omni-AD.

C. Ablation Studies

This section analyzes the component effectiveness in our design. All experiments are done on the MVTec-AD dataset.

Effect of learnable tokens. Table II studies the role of learnable tokens. As shown, when learnable tokens are absent (row-1), *i.e.*, using plain self-attention, the performance only reaches 54.0 AP at pixel-level. When replacing the query with learnable tokens, we increase this metric to 56.6 (+2.6%). All the other metrics are also improved. Further replacing key and value with learnable keys (row 3) can consistently augment both anomaly detection and localization on 6/7 metrics, with comparable AU-ROC at pixel level, demonstrating the effectiveness of replacing both Q and KV with learnable tokens.

Effect of learnable tokens position. Table III studies the impact of replacing Q and KV with learnable tokens in various orders, denoted as A+B for replacements. While these changes have a minor impact on detection performance, *they significantly influence localization performance*. The Q+KV combination achieves the best results in both aspects across 6 metrics, making it as the default configuration.

Effect of learnable token numbers. Table IV shows our method is robust to the number of learnable tokens. Setting it to 64 achieves the best performance with comparable complexity, making it the default choice.

Effect of local and global branch. As shown in Table V, when the local branch is disabled, the model's detection capability decreases, but it maintains good localization ability, reaching 93.0% AU-PRO. When the global branch is disabled, the model still retains strong detection performance, but its localization ability significantly decreases, leading to an AU-PRO reduction of 2.6%. This indicates that the global branch plays a crucial role in anomaly localization, while the local branch significantly enhances detection performance.

TABLE I
PERFORMANCE COMPARISONS (%) WITH STATE-OF-THE-ARTS ON DIFFERENT AD DATASETS FOR MULTI-CLASS SETTING.

Dataset	Method	Source	Image-level			Pixel-level				mAD
			AU-ROC	AP	F1_max	AU-ROC	AP	F1_max	AU-PRO	
MVTec-AD [6]	RD4AD [29]	CVPR'22	94.6	96.5	95.2	96.1	48.6	53.8	91.1	82.3
	UniAD [3]	NeurIPS'22	96.5	98.8	96.2	96.8	43.4	49.5	90.7	81.7
	SimpleNet [4]	CVPR'23	95.3	98.4	95.8	96.9	45.9	49.7	86.5	81.2
	DeSTSeg [30]	CVPR'23	89.2	95.5	91.6	93.1	54.3	50.9	64.8	77.1
	DiAD [19]	AAAI'24	97.2	99.0	96.5	96.8	52.6	55.5	90.7	84.0
	RLR [8]	ECCV'24	98.6	-	-	98.5	-	-	-	-
	MambaAD [5]	NeurIPS'24	98.6	99.6	97.8	97.7	56.3	59.2	93.1	86.0
	Omni-AD	-	99.0	99.7	98.3	97.9	56.8	59.9	93.4	86.4
VisA [24]	RD4AD [29]	CVPR'22	92.4	92.4	89.6	98.1	38.0	42.6	91.8	77.8
	UniAD [3]	NeurIPS'22	88.8	90.8	85.8	98.3	33.7	39.0	85.5	74.6
	SimpleNet [4]	CVPR'23	87.2	87.0	81.8	96.8	34.7	37.8	81.4	72.4
	DeSTSeg [30]	CVPR'23	88.9	89.0	85.2	96.1	39.6	43.4	67.4	72.8
	DiAD [19]	AAAI'24	86.8	88.3	85.1	96.0	26.1	33.0	75.2	70.1
	MambaAD [5]	NeurIPS'24	94.3	94.5	89.4	98.5	39.4	44.0	91.0	78.7
		Omni-AD	-	94.6	95.0	90.3	98.8	38.7	43.3	91.9
Real-IAD [25]	UniAD [3]	NeurIPS'22	83.0	80.9	74.3	97.3	21.1	29.2	86.7	67.5
	SimpleNet [4]	CVPR'23	57.2	53.4	61.5	75.7	2.8	6.5	39.0	42.3
	DeSTSeg [30]	CVPR'23	82.3	79.2	73.2	94.6	37.9	41.7	40.6	64.2
	DiAD [19]	AAAI'24	75.6	66.4	69.9	88.0	2.9	7.1	58.1	52.6
	MambaAD [5]	NeurIPS'24	86.3	84.6	77.0	98.5	33.0	38.7	90.5	72.7
		Omni-AD	-	88.2	86.5	79.1	98.8	34.3	39.7	91.6

TABLE II
ABLATION STUDY OF LEARNABLE Q AND KV.

Q	KV	Image-level			Pixel-level			
		AU-ROC	AP	F1_max	AU-ROC	AP	F1_max	AU-PRO
-	-	98.4	99.4	97.8	97.6	54.0	57.6	91.9
✓		98.6	99.5	98.2	98.0	56.6	59.7	93.1
✓	✓	99.0	99.7	98.3	97.9	56.8	59.9	93.4

TABLE III
ABLATION STUDY OF THE COMBINATION OF LEARNABLE Q AND K, V.

Combination	Image-level			Pixel-level			
	AU-ROC	AP	F1_max	AU-ROC	AP	F1_max	AU-PRO
Q + Q	99.0	99.7	98.4	98.0	55.0	59.0	92.9
KV + KV	98.9	99.6	98.4	97.7	51.2	56.6	91.4
KV + Q	99.0	99.7	98.4	98.0	55.4	59.1	93.0
Q + KV	99.0	99.7	98.3	97.9	56.8	59.9	93.4

Effect of decoder depth at each stage. Table VI shows that increasing the decoder depth improves performance but also raises computational complexity and parameter overhead. A depth of 3-9-9-7 offers the best results with a manageable increase in complexity, making it our default configuration.

Effect of backbones. Table VII shows that using ResNet34 as the backbone achieves the highest performance and remarkable efficiency compared to others. ResNet18 is an excellent choice for prioritizing efficiency.

Visualization. Figure 3 visualize results on MVTec-AD and VisA. Our framework successfully detects the visual anomalies of diverse structures and appearances across various objects more precisely, demonstrating its strong capacity.

V. CONCLUSION AND FUTURE WORK

We propose Omni-AD for multi-class unsupervised anomaly detection, which consists of a pre-trained encoder, a feature

TABLE IV
ABLATION STUDY OF THE NUMBER OF LEARNABLE TOKENS.

Number	Params(M)	FLOPs(G)	mAD
16	29.4	10.1	86.2
36	29.6	10.5	86.2
64	29.9	11.2	86.4
100	30.3	12.0	86.2

TABLE V
ABLATION STUDY OF GLOBAL AND LOCAL BRANCHES.

Global	Local	Image-level			Pixel-level			
		AU-ROC	AP	F1_max	AU-ROC	AP	F1_max	AU-PRO
✓	×	98.1	99.3	97.5	97.8	56.1	59.1	93.0
×	✓	98.8	99.6	98.2	97.4	49.3	55.6	90.8
✓	✓	99.0	99.7	98.3	97.9	56.8	59.9	93.4

TABLE VI
ABLATION STUDY OF DECODER DEPTH AT EACH STAGE.

Depths	Params(M)	FLOPs(G)	mAD
2-2-2-2 (8)	19.0	6.3	85.1
3-6-6-3 (18)	26.5	8.7	86.2
3-9-9-7 (28)	29.9	11.2	86.4
6-12-11-9 (38)	42.7	13.7	86.3

TABLE VII
ABLATION STUDY ON RESNET SERIES ENCODERS

Encoder	Params(M)	FLOPs(G)	mAD
ResNet18	24.5	9.0	85.9
ResNet34	29.9	11.2	86.4
ResNet50	468	114	85.5
WideResNet50	484	121	86.3

fusion neck, and a decoder that learns to reconstruct multi-scale normal features from local and global perspectives. At the core of our decoder, a two-branch block named Omni is

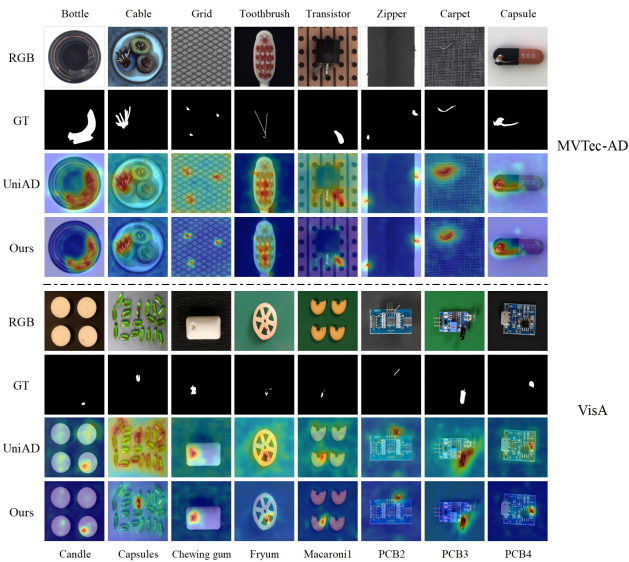


Fig. 3. Qualitative results on MVTEc and VisA.

introduced. It has a local branch learning normal features of local granularity with depth-convolution layers. The remaining global branch captures normal patterns with learnable tokens. Omni-AD has attained outstanding performance on public AD benchmarks. In the future, we plan to extend it to other domains, such as medical imaging, to demonstrate its generality.

VI. ACKNOWLEDGMENT

This work is supported by Hubei Province Natural Science Foundation (No.2023AFB267); National Natural Science Foundation of China (No.62302188); Fundamental Research Funds for the Central Universities (No.2662023XXQD001).

REFERENCES

- [1] Karsten Roth, Latha Pemula, Joaquin Zepeda, Bernhard Schölkopf, Thomas Brox, and Peter Gehler, "Towards total recall in industrial anomaly detection," in *CVPR*, 2022, pp. 14318–14328.
- [2] Vitjan Zavrtanik, Matej Kristan, and Danijel Škočaj, "Draem-a discriminatively trained reconstruction embedding for surface anomaly detection," in *ICCV*, 2021, pp. 8330–8339.
- [3] Zhiyuan You, Lei Cui, Yujun Shen, Kai Yang, Xin Lu, Yu Zheng, and Xinyi Le, "A unified model for multi-class anomaly detection," *NeurIPS*, vol. 35, pp. 4571–4584, 2022.
- [4] Zhikang Liu, Yiming Zhou, Yuansheng Xu, and Zilei Wang, "Simplenet: A simple network for image anomaly detection and localization," in *CVPR*, 2023, pp. 20402–20411.
- [5] Haoyang He, Yuhu Bai, Jiangning Zhang, Qingdong He, Hongxu Chen, Zhenye Gan, Chengjie Wang, Xiangtai Li, Guanzhong Tian, and Lei Xie, "Mambaad: Exploring state space models for multi-class unsupervised anomaly detection," in *NeurIPS*, 2024, vol. 37, pp. 71162–71187.
- [6] Paul Bergmann, Michael Fauser, David Sattlegger, and Carsten Steger, "Mvtec ad—a comprehensive real-world dataset for unsupervised anomaly detection," in *CVPR*, 2019, pp. 9592–9600.
- [7] Ashish Vaswani, Noam Shazeer, Niki Parmar, Jakob Uszkoreit, Llion Jones, Aidan N Gomez, Łukasz Kaiser, and Illia Polosukhin, "Attention is all you need," *NeurIPS*, vol. 30, 2017.
- [8] Liren He, Zhengkai Jiang, Jinlong Peng, Wenbing Zhu, Liang Liu, Qiangang Du, Xiaobin Hu, Mingmin Chi, Yabiao Wang, and Chengjie Wang, "Learning unified reference representation for unsupervised multi-class anomaly detection," in *ECCV*, 2024, pp. 216–232.
- [9] Jiawei Yu, Ye Zheng, Xiang Wang, Wei Li, Yushuang Wu, Rui Zhao, and Liwei Wu, "Fastflow: Unsupervised anomaly detection and localization via 2d normalizing flows," *arXiv preprint arXiv:2111.07677*, 2021.

- [10] Thomas Defard, Aleksandr Setkov, Angélique Loesch, and Romaric Audigier, "Padim: a patch distribution modeling framework for anomaly detection and localization," in *ICPR*, 2021, pp. 475–489.
- [11] Chun-Liang Li, Kihyuk Sohn, Jinsung Yoon, and Tomas Pfister, "Cut-paste: Self-supervised learning for anomaly detection and localization," in *CVPR*, 2021, pp. 9664–9674.
- [12] Yuxuan Cai, Dingkan Liang, Dongliang Luo, Xinwei He, Xin Yang, and Xiang Bai, "A discrepancy aware framework for robust anomaly detection," *IEEE TII*, 2023.
- [13] Nicolae-Cătălin Ristea, Neelu Madan, Radu Tudor Ionescu, Kamal Nasrollahi, Fahad Shahbaz Khan, Thomas B Moeslund, and Mubarak Shah, "Self-supervised predictive convolutional attentive block for anomaly detection," in *CVPR*, 2022, pp. 13576–13586.
- [14] Xudong Yan, Huaidong Zhang, Xuemiao Xu, Xiaowei Hu, and Pheng-Ann Heng, "Learning semantic context from normal samples for unsupervised anomaly detection," in *AAAI*, 2021, vol. 35, pp. 3110–3118.
- [15] Julian Wyatt, Adam Leach, Sebastian M Schmon, and Chris G Willcocks, "Anoddp: Anomaly detection with denoising diffusion probabilistic models using simplex noise," in *CVPR*, 2022, pp. 650–656.
- [16] Pankaj Mishra, Riccardo Verk, Daniele Fornasier, Claudio Piciarelli, and Gian Luca Foresti, "Vt-adl: A vision transformer network for image anomaly detection and localization," in *2021 IEEE 30th International Symposium on Industrial Electronics (ISIE)*, 2021, pp. 01–06.
- [17] Ying Zhao, "Omnia: A unified cnn framework for unsupervised anomaly localization," in *CVPR*, 2023, pp. 3924–3933.
- [18] Ruiying Lu, YuJie Wu, Long Tian, Dongsheng Wang, Bo Chen, Xiyang Liu, and Ruimin Hu, "Hierarchical vector quantized transformer for multi-class unsupervised anomaly detection," *NeurIPS*, vol. 36, pp. 8487–8500, 2023.
- [19] Haoyang He, Jiangning Zhang, Hongxu Chen, Xuhai Chen, Zhishan Li, Xu Chen, Yabiao Wang, Chengjie Wang, and Lei Xie, "A diffusion-based framework for multi-class anomaly detection," in *AAAI*, 2024, pp. 8472–8480.
- [20] Jia Deng, Wei Dong, Richard Socher, Li-Jia Li, Kai Li, and Li Fei-Fei, "Imagenet: A large-scale hierarchical image database," in *CVPR*, 2009, pp. 248–255.
- [21] Kaiming He, Xiangyu Zhang, Shaoqing Ren, and Jian Sun, "Deep residual learning for image recognition," in *CVPR*, 2016, pp. 770–778.
- [22] Mingxing Tan and Quoc Le, "Efficientnet: Rethinking model scaling for convolutional neural networks," in *ICML*, 2019, pp. 6105–6114.
- [23] Golnaz Ghiasi, Tsung-Yi Lin, and Quoc V Le, "Nas-fpn: Learning scalable feature pyramid architecture for object detection," in *CVPR*, 2019, pp. 7036–7045.
- [24] Yang Zou, Jongheon Jeong, Latha Pemula, Dongqing Zhang, and Onkar Dabeer, "Spot-the-difference self-supervised pre-training for anomaly detection and segmentation," in *ECCV*, 2022, pp. 392–408.
- [25] Chengjie Wang, Wenbing Zhu, Bin-Bin Gao, Zhenye Gan, Jiangning Zhang, Zhihao Gu, Shuguang Qian, Mingang Chen, and Lizhuang Ma, "Real-iaad: A real-world multi-view dataset for benchmarking versatile industrial anomaly detection," in *CVPR*, 2024, pp. 22883–22892.
- [26] Jiangning Zhang, Haoyang He, Zhenye Gan, Qingdong He, Yuxuan Cai, Zhucun Xue, Yabiao Wang, Chengjie Wang, Lei Xie, and Yong Liu, "Ader: A comprehensive benchmark for multi-class visual anomaly detection," *arXiv preprint arXiv:2406.03262*, 2024.
- [27] Paul Bergmann, Michael Fauser, David Sattlegger, and Carsten Steger, "Uninformed students: Student-teacher anomaly detection with discriminative latent embeddings," in *CVPR*, 2020, pp. 4183–4192.
- [28] Jiangning Zhang, Xuhai Chen, Yabiao Wang, Chengjie Wang, Yong Liu, Xiangtai Li, Ming-Hsuan Yang, and Dacheng Tao, "Exploring plain vit features for multi-class unsupervised visual anomaly detection," *CVIU*, vol. 253, pp. 104308, 2025.
- [29] Hanqiu Deng and Xingyu Li, "Anomaly detection via reverse distillation from one-class embedding," in *CVPR*, 2022, pp. 9737–9746.
- [30] Xuan Zhang, Shiyu Li, Xi Li, Ping Huang, Jiulong Shan, and Ting Chen, "Destseg: Segmentation guided denoising student-teacher for anomaly detection," in *CVPR*, 2023, pp. 3914–3923.